Available online at www.sciencedirect.com
ScienceDirect
Trans. Nonferrous Met. Soc. China 28(2018) 1061−1072
Transactions of Nonferrous Metals Society of China
www.tnmsc.cn

Effect of Si addition and applied pressure on microstructure and tensile properties of as-cast Al−5.0Cu−0.6Mn−1.2Fe alloys

Wei-wen ZHANG, Yu-liang ZHAO, Da-tong ZHANG, Zong-qiang LUO, Chao YANG, Yuan-yuan LI

National Engineering Research Center of Near-net-shape Forming for Metallic Materials, South China University of Technology, Guangzhou 510641, China

Received 29 January 2017; accepted 22 May 2017

Abstract: The effects of Si addition and applied pressure on the microstructure and tensile properties of as-cast Al−5.0Cu−0.6Mn−1.2Fe alloys were studied. The results show that Si addition promotes the formation of Chinese script α-Fe, and suppresses the precipitation of Al_3(FeMn) and Al_6(FeMn). For the alloys produced without pressure, Si addition increases the volume fraction of porosity, resulting in remarkable decrease in ultimate tensile strength (UTS) and yield strength (YS). For the alloys produced with 75 MPa pressure, Si addition improves UTS and YS owing to the formation of high number density of Al_2Cu (θ) phases. The tensile properties of alloys increase with increasing applied pressure at the same Si content level, which is attributed to elimination of porosity, grain refinement strengthening and solid-solution strengthening. The alloy with 1.1% Si addition and 75 MPa pressure shows the best tensile properties, where the UTS, YS and elongation are 237 MPa, 140 MPa and 9.8%, respectively.
Key words: Al−Cu alloys; Si addition; solidification; tensile properties; microstructure

1 Introduction

Cast aluminum alloys, due to their low density and excellent mechanical properties, have been widely used in transportation and aerospace areas, particularly for production of automotive components [1−3]. In addition, recycled Al alloys have received considerable attention since only 3% of the energy is required compared with the primary production from natural resources [4]. However, one of the greatest challenges to Al recycling is the high impurity elements in the scraps [5]. Fe is one of the most common impurities in commercial Al alloys, and the Fe levels in the alloys can be invariably increased with the accumulation. However, in the Al−Cu alloys, extremely low Fe content is required, for example, less than 0.10% (mass fraction) Fe in A206 series alloys [6]. The solid-state solubility of Fe in α(Al) is about 0.05% (mass fraction) in equilibrium state [7] and it is even less under real solidification conditions. Consequently, Fe in Al−Cu alloys usually precipitates in the form of the Fe-rich intermetallics, including Al_3(FeMn) [8,9], Al_6(FeMn) [10,11], Al_m(FeMn) [8,11], Al_7Cu_2Fe (β-Fe) [12−14] and $Al_{15}(FeMn)_3(SiCu)_2$ (α-Fe) [15,16]. Among these Fe-rich intermetallics, the plate-like Al_3(FeMn) and β-Fe could severely deteriorate the tensile properties of the alloys due to their brittle nature which could result in the crack initiation and propagation [17]. Compared with the coarse plate-like Al_3(FeMn) and β-Fe, the Fe-rich intermetallic in the form of compact Chinese script has been found to be less harmful to tensile properties [18]. Mn is the most commonly used alloying element to neutralize the effect of Fe and modify the plate-like Fe-rich intermetallics into less harmful morphologies [19].

Si, like Fe, is another major impurity in many high strength commercial Al−Cu alloys [1]. Recently, interesting research findings [1,15,20−23] have been reported concerning Si transferring the Fe-rich intermetallics from platelet-like to less harmful Chinese script. LIU et al [8,20,21] proposed that the addition of Si is helpful to promote the formation of α-Fe and hinder the precipitation of β-Fe because the formation temperature of α-Fe is higher than that of β-Fe and there

Foundation item: Project (51374110) supported by the National Natural Science Foundation of China, Project (2015B090926004) supported by Science and Technology Program of Guangdong Province, China; Project (2015A030312003) supported by the Natural Science Foundation of Guangdong Province, China
Corresponding author: Wei-wen ZHANG; Tel: +86-20-87112022; Fax: +86-20-87112111; E-mail: mewzhang@scut.edu.cn
DOI: 10.1016/S1003-6326(18)64765-X

are less free Fe atoms available for the formation of β-Fe. KAMGA et al [22,23] further confirmed this result. However, TALAMANTES-SILVA et al [24] reported that β-Fe is the only Fe-rich intermetallic in the 206 alloys with Si/Fe ratio of 1 and Mn/Fe ratio of 3.5. LEMIEUX et al [25] and HAN et al [26] observed that the addition of Si does not have an effect on the strength, but decreases the ductility of the alloys. However, there are controversial results about the effect of Si on the Al−Cu alloys, i.e., whether Si is an impurity or a beneficial alloying element, or in which range that Si can improve the mechanical properties in Al−Cu alloys. Therefore, it is vital to study the effect of Si on the microstructure evolution and tensile properties of recycled Al−Cu alloys with high Fe and Si contents.

Squeeze casting is a technology with short route, high efficiency and precise forming, possessing features of casting and plastic processing [13,27−29], which offers advantages such as enhancing the cooling rate and eliminating casting defects of porosity and shrinkage. Recently, LI et al [28] reported that squeeze casting could greatly improve the performance of light alloys and reduce the impurity restriction in recycling material. In our previous studies [13,16,30,31], we reported that squeeze casting decreases the secondary dendritic arm spacing (SDAS) of α(Al) and the porosity and significantly affects the intermetallics, such as Fe-rich intermetallics, in Al−Cu alloys.

With accumulation of recycled Al−Cu alloys scraps, the content of Fe and Si elements is relatively high. However, previous studies were mainly focused on the effect of low content of Fe and Si element on the Al−Cu alloys. In the present work, the microstructure and tensile properties of Al−Cu alloys with high contents of Fe and Si were studied during squeeze casting produced by casting with or without pressure.

2 Experimental

The alloys with various Si contents were produced by melting commercially pure Al (99.5%) and the master alloys of Al−50%Cu, Al−10%Mn, Al−20%Si and Al−5%Fe. The real chemical composition was analyzed by optical emission spectrometer, as given in Table 1. Firstly, 10 kg raw materials were melted at about 730 °C in a clay-graphite crucible using an electric resistance furnace and the melts were degassed by 0.5% C_2Cl_6 to minimize hydrogen content. The pouring temperature was set to be 710 °C after degassing and the die was preheated to ~200 °C before squeeze casting. After the melt was poured into a cylindrical die, varied pressure (0, 25 and 75 MPa) was applied to melts and held for 30 s until the melt was completely solidified. Finally, the ingots with sizes of d 65 mm × 68 mm were obtained.

Table 1 Chemical compositions of experimental alloys (mass fraction, %)

Alloy	Cu	Mn	Fe	Si	Al
Al−5.0Cu−0.6Mn−1.2Fe−0Si	5.19	0.64	1.22	0.03	Bal.
Al−5.0Cu−0.6Mn−1.2Fe−0.15Si	5.30	0.63	1.22	0.17	Bal.
Al−5.0Cu−0.6Mn−1.2Fe−0.55Si	5.23	0.63	1.22	0.58	Bal.
Al−5.0Cu−0.6Mn−1.2Fe−1.1Si	5.05	0.67	1.29	1.09	Bal.

The tensile samples with dimensions of d 10 mm × 65 mm were cut from the edge of the ingots. Tensile tests were carried out at room temperature using a SANS CMT5105 standard testing machine with a strain rate of 1 mm/min. At least three samples were tested to obtain the average value. Samples for metallographic observation were cut from the end of tensile specimens. Metallographic samples were etched with 0.5% HF solution for 30 s. Samples for grain size measurement were examined in Leica optical microscope with polarized light after anodizing with a 4% HBF_4 solution for about 30 s at 20 V. The random linear intercept technique was used in the center of the samples to measure the grain size and 20 images were used to calculate the grain size. The microstructure was analyzed with the image analysis software Leica materials workstation V3.6.1. The area fractions of intermetallics were calculated based on the assumption that the morphology of the intermetallics is uniform. Nearly 50 different fields were examined for each sample. The average chemical compositions of the phases and fracture surfaces of tensile specimens were analyzed using SEM Quanta 200, energy-dispersive X-ray analyzer (EDX) and EPMA−1600 electron probe micro-analyzer. X-ray diffractometer (Bruker D8 ADVANCE) was used to further index these phases, which was operated at 40 kV and 100 mA. The morphology of the Fe-rich intermetallics was further studied by transmission electron microscopy (TEM) using a Philips microscope (FEI 3010). Cu content in the α(Al) matrix in the as-cast state was measured by EPMA−1600 electron probe micro-analyzer.

3 Results and discussion

3.1 Microstructure

The grain size distributions of the 0% Si alloys with and without applied pressure after anodizing are displayed in Fig. 1. The red line in Fig. 1 is marked in order to distinguish different grains on the grain boundary. It can be seen that the grain size of the alloy produced with 75 MPa applied pressure is smaller than that of the alloy produced without applied pressure. The statistics results (Fig. 1(c)) show that the increase of applied pressure results in a grain size reduction. The

measured SDAS of α(Al) decreases from ~80 μm for the alloy without applied pressure to ~30 μm for the alloy with 75 MPa applied pressure. The reduction in grain size is mainly attributed to the applied pressure which can reduce the air gap between the melt and die and an associated increase in the cooling rate, leading to local high undercooling and the increased nucleation rate of primary α(Al) [27].

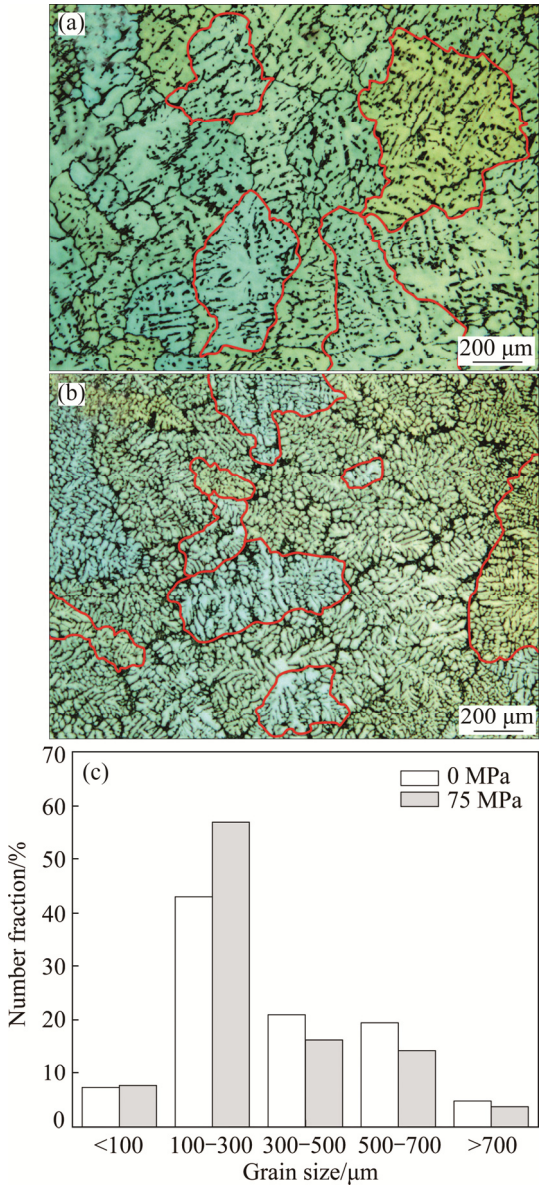

Fig. 1 Effect of applied pressure on grain size of alloy containing 0% Si: (a) Without applied pressure; (b) With 75 MPa applied pressure; (c) Histogram showing distribution of grain size of alloy with and without applied pressure

Figure 2 shows the corresponding microstructure of Al−5.0Cu−0.6Mn−1.2Fe alloys with Si content varying from 0% to 1.1% without applied pressure. As can be seen, the microstructure consists of the primary α(Al), Al_2Cu, platelet-like Al_3(FeMn), Chinese script Al_6(FeMn) and α-Fe, confirmed by the EDS results (Table 2). The irregular-shaped light grey phase observed in the microstructure is Al_2Cu, which is obtained from the eutectic reaction during solidification. These Fe-rich intermetallics are typical phases found in Al−Cu alloys [8,13,32]. As seen from Fig. 2(a), the platelet-like Al_3(FeMn) and Chinese script Al_6(FeMn) precipitates are the main Fe-rich intermetallics in the alloys without Si addition. There is only a little morphology change when the Si content is raised from 0% to 0.15% (Fig. 2(b)). In the alloy with 0.55% Si, Chinese script α-Fe and Al_6(FeMn) coexist (Fig. 2(c)), while only Chinese script α-Fe is presented when Si content is further increased to 1.1% (Fig. 2(d)). These indicate that Si promotes the formation of α-Fe and suppresses the formation of Al_3(FeMn) and Al_6(FeMn) phases. Compared with the alloys without applied pressure, the applied pressure influences both the size and morphology of the α(Al) and secondary intermetallics. As shown in Fig. 3, the morphology of Fe-rich intermetallics is smaller and more compact in the sample with applied pressure of 75 MPa.

As shown in Fig. 4, the volume fraction of porosities in the alloys with 1.1% Si is higher than that in the alloys with 0% Si. Moreover, the size of the Fe-rich intermetallics without applied pressure is obviously larger than that of intermetallics with applied pressure.

The DSC heating curves of Al−5.0Cu−0.6Mn−1.2Fe alloys with different Si contents are presented in Fig. 5. The DSC curve of the alloy with 0% Si exhibits three distinct endothermic peaks at 656.9, 603.0 and 551 °C, corresponding to the melting of the primary α(Al) phases, Chinese script Al_6(FeMn) phases, and eutectic Al_2Cu phases, respectively. Similarly, the DSC curve of the alloy with 1.1% Si exhibits three distinct endothermic peaks at 649.6, 535.2 and 525.5 °C, corresponding to the melting of the primary α(Al) phases, eutectic Al_2Cu phases, and eutectic Si phases, respectively. With increasing Si content, the endothermic peaks of Al_6(FeMn) phase disappear, which is consistent with the microstructure (Fig. 2). With increasing Si content, the temperature of liquid and formation of phase is reduced. These results are in agreement with Refs. [20,23], which indicates that the precipitation temperature of the blocky Al_2Cu phase is lowered.

The quantitative analysis results of volume fraction of secondary intermetallics and porosity as a function of Si content are shown in Fig. 6. These results indicate that the volume fraction of Fe-rich intermetallics depends on the Si content and applied pressure. The volume fraction of the total secondary intermetallics, Chinese Fe-rich intermetallics and porosity increases with increasing Si content, while the volume fraction of platelet-like Fe-rich intermetallics and Al_2Cu decreases with increasing Si content.

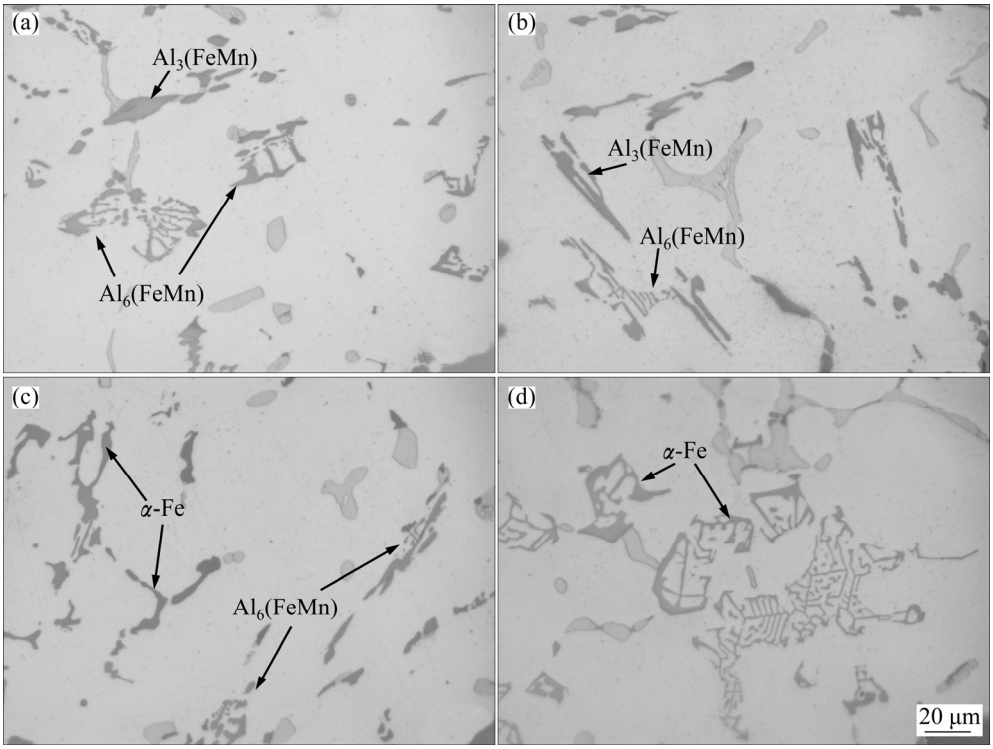

Fig. 2 Microstructures of as-cast alloys at applied pressure of 0 MPa: (a) 0% Si; (b) 0.15% Si; (c) 0.55% Si; (d) 1.1% Si

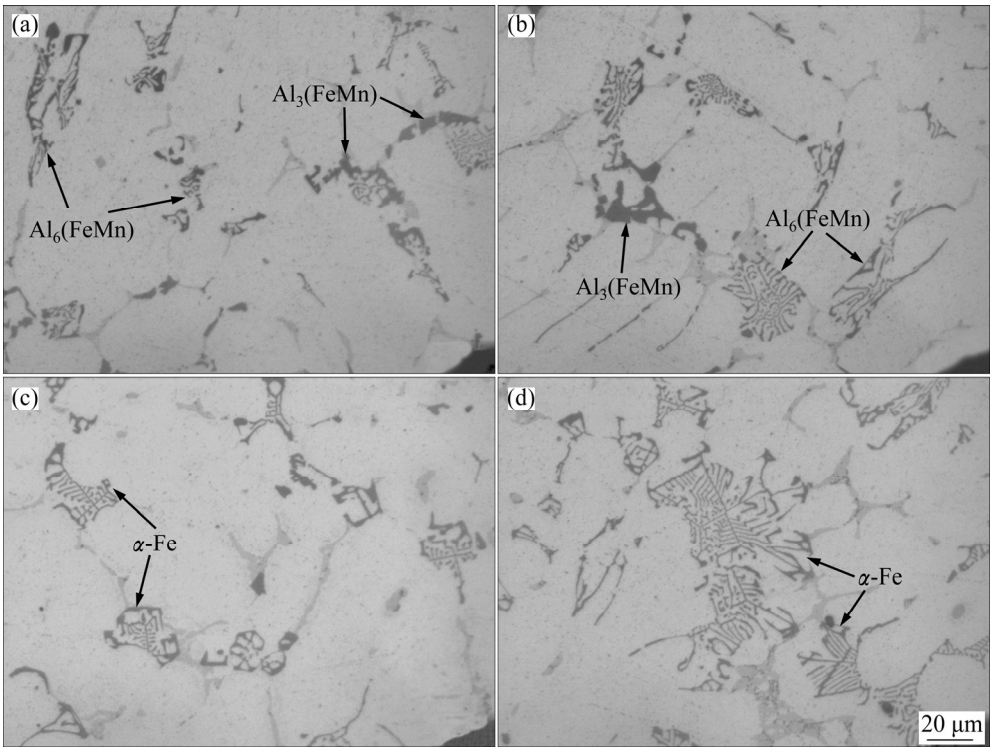

Fig. 3 Microstructures of as-cast alloys at applied pressure of 75 MPa: (a) 0% Si; (b) 0.15% Si; (c) 0.55% Si; (d) 1.1% Si

Table 2 Average composition of secondary intermetallics (molar fraction, %)

Phase	Al	Cu	Mn	Fe	Si
Al_2Cu	65.61±1.41	34.39±1.41	−	−	−
$Al_3(FeMn)$	75.01±1.94	5.24±1.38	3.65±0.74	16.10±1.55	−
$Al_6(FeMn)$	82.77±2.12	4.50±1.29	2.35±0.56	10.38±1.22	−
$Al_{15}(FeMn)_3(CuSi)_2$	75.30±3.91	2.68±0.24	4.17±1.00	12.84±2.59	5.01±0.30

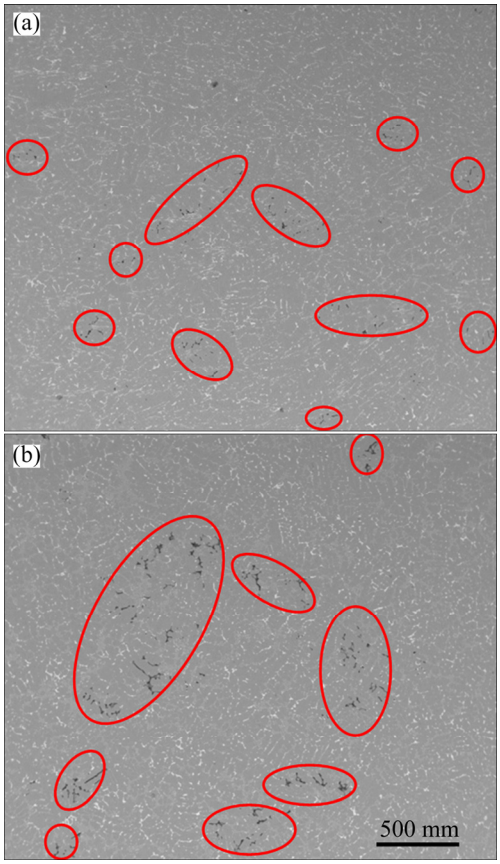

Fig. 4 Porosities in alloys at low magnification: (a) 0% Si; (b) 1.1% Si

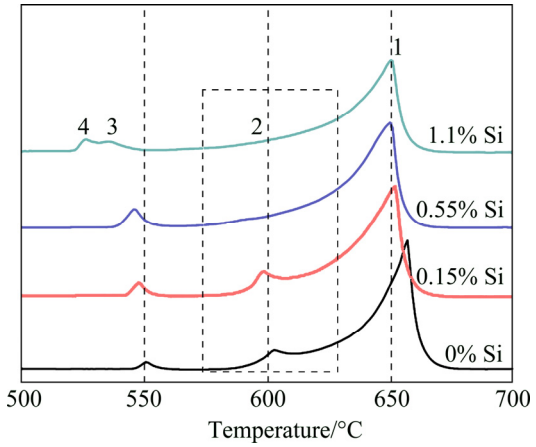

Fig. 5 DSC heating curves of alloys with different Si contents

Figure 7 shows the TEM bright-field images of the morphology and distribution of the θ phases in the alloys with different Si contents prepared with applied pressure of 75 MPa. The coarse and needle-like θ phases (~800 nm) are uniformly distributed in the α(Al) matrix without Si addition (Fig. 7(a)). With 1.1% Si addition, the size of θ phases is remarkably refined to ~100 nm (Fig. 7(b)) and its EDX result is shown in Fig. 7(c). This indicates that the Si addition promotes the precipitation of high number density θ phases in the alloys and reduces their size. The similar phenomenon was also detected in the Al−Sc−Si [33] and Al−Cu−Si [34] alloys. They considered that the addition of Si could promote the heterogeneous nucleation of the precipitates. The main reason is that Si could retard the coarsening of θ precipitates and catalyze the heterogeneous nucleation of θ. The Si addition enhances the solubility of Cu in Al, which means less undercooling and lower driving force for the precipitation [34]. In the meantime, Cu could retard the nucleation of Si in the Al−Cu−Si alloys. Once the Si precipitates are formed, they catalyze the nucleation of θ. Si precipitates provide a higher density distribution of heterogeneous nucleation sites, resulting in the precipitation of smaller size θ phase [34]. The other reason is that Si substitutes Cu in the α-Fe ($Al_{15}(FeMn)_3(SiCu)_2$), meaning that there are more Cu atoms available for formation of θ phase.

Figure 8 represents the TEM microstructure and selected area diffraction patterns (SADP) of the alloys with different Si contents and applied pressure. Figure 8(a) shows that the platelet-like $Al_3(FeMn)$ with the width of 2 μm is adjacent to Al_2Cu in the matrix. The $Al_3(FeMn)$ has a monoclinic structure with lattice constants of a=1.549 nm, b=0.808 nm and c=1.248 nm. These features are in accordance with the previous works [8,18]. The Chinese script phase is identified as $Al_6(FeMn)$ in Fig. 8(b), which has an orthorhombic structure and lattice parameters of a=0.643 nm, b=0.746 nm and c=0.878 nm. Figure 8(c) manifests the morphology of α-Fe in alloys produced without applied pressure at 1.1% Si. From the SAED pattern analysis, the α-Fe phase, with a body-centered cubic structure, is found to have the lattice parameters of $a=b=c$=1.265 nm. This phase is also observed in the Al−Si alloy [35].

Figure 9 shows the SEM images of samples after deep-etching, revealing the three-dimensional morphologies of Fe-rich intermetallics. The typical morphology of the deep-etched $Al_3(FeMn)$ phase is long platelet with some branches (Fig. 9(a)). The Chinese script $Al_6(FeMn)$ phase shows a three-dimensional compact skeletal structure (Fig. 9(b)). Figure 9(c) shows the typical eutectic structures of α-Fe with fishbone shape, which is consistent with the previous work [7]. The primary branches grow from center to the side and the secondary branches can grow directly from the sides of the large primary axes. SEM−EDS mapping shown in Fig. 10 reveals that the Si and Mn elements exist not only in the α-Fe phase but also in α(Al) matrix. This also indicates that the grey and long branch phase is Fe-rich intermetallics phase.

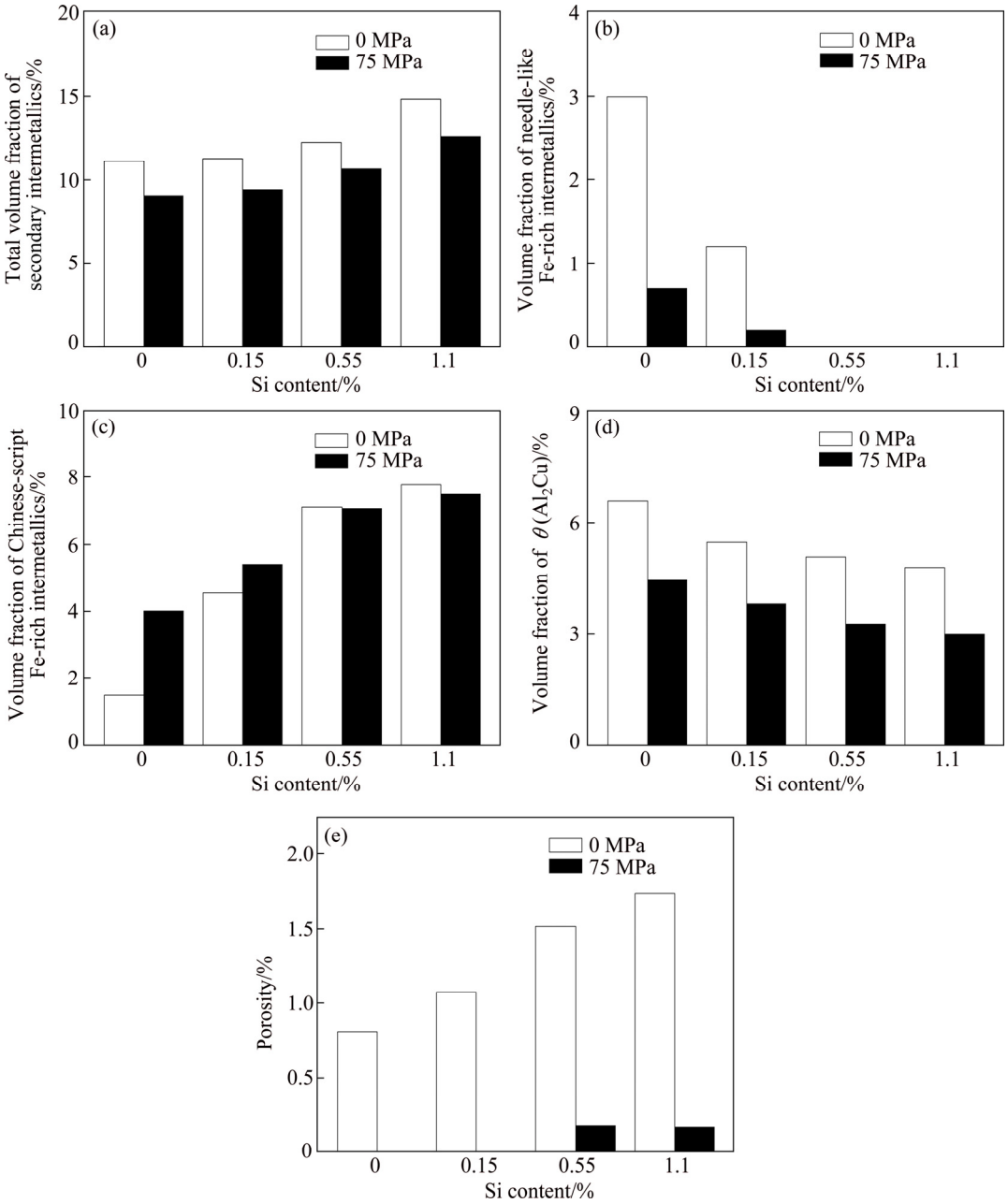

Fig. 6 Microstructural features of alloys with different applied pressures and Si contents: (a) Total volume fraction of secondary intermetallics; (b) Volume fraction of needle-like Fe-rich intermetallics; (c) Volume fraction of Chinese-script Fe-rich intermetallics; (d) Volume fraction of θ (Al_2Cu); (e) Porosity

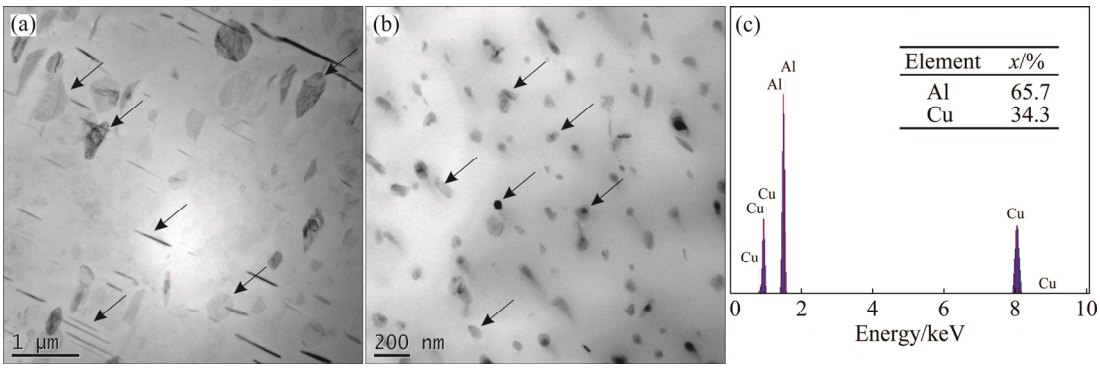

Fig. 7 TEM micrographs of alloys produced by applied pressure of 75 MPa without (a) and with 1.1% Si addition (b) and EDS analysis results of Al_2Cu (c)

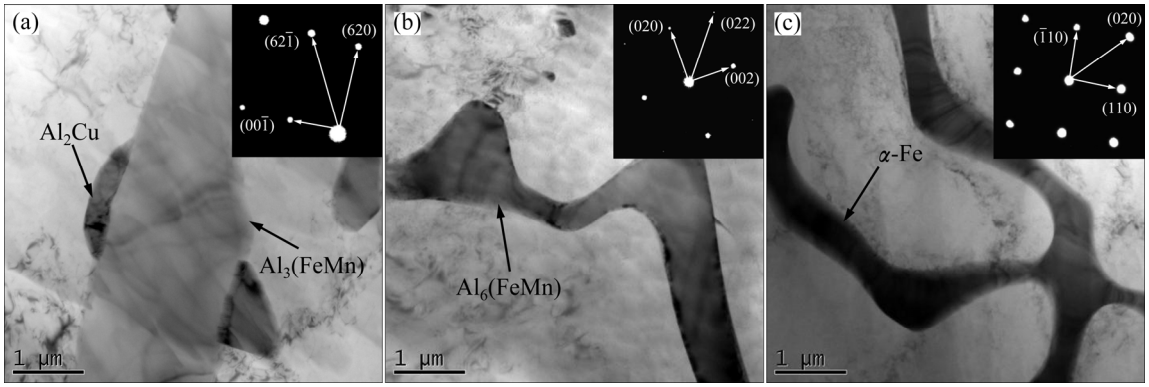

Fig. 8 Microstructures of experimental samples examined by TEM: (a) $Al_3(FeMn)$; (b) $Al_6(FeMn)$; (c) α-Fe

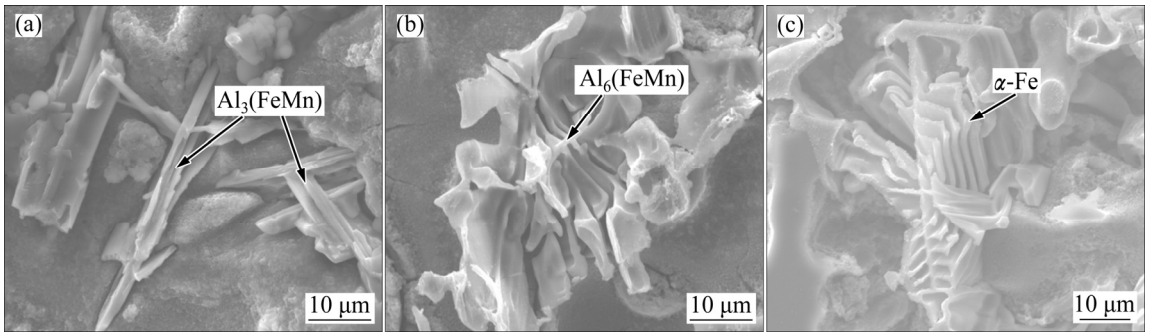

Fig. 9 Typical three-dimensional morphologies of Fe-rich intermetallics: (a) Platelet $Al_3(FeMn)$; (b) Chinese script $Al_6(FeMn)$; (c) Chinese script α-Fe

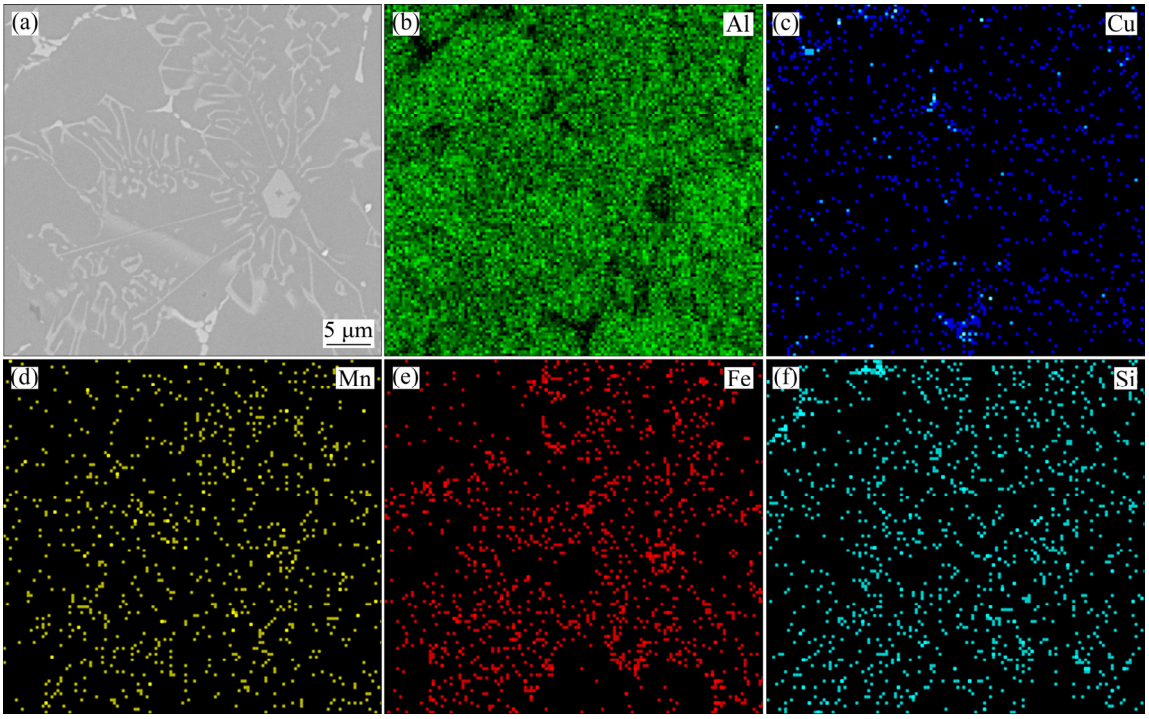

Fig. 10 Elemental distributions of α-Fe phase: (a) Morphology; (b) Al; (c) Cu; (d) Mn; (e) Fe; (f) Si

The promotion effect of Si on the formation of α-Fe can be summarized as follows. Firstly, Si could react with Mn and Fe to form α-Fe when the enough amounts of these alloying elements exist in the alloy [20,36]. Secondly, the growth rate of monoclinic structure $Al_3(FeMn)$ and orthorhombic structure $Al_6(FeMn)$ is

slower than that of the body-centered cubic structure α-Fe [8]. Since the presence of Si has a strong restriction effect [22], which is helpful to the formation of compact and cubic α-Fe and suppresses the formation of two-dimensional plate-like $Al_3(FeMn)$, α-Fe can nucleate and grow quickly on the three-dimensional network of dendrite arm (Fig. 8(c)) in any direction [8]. Thirdly, increasing Si content reduces the liquidus temperature (Fig. 4), resulting in the easy formation of α-Fe, because the formation temperature of $Al_3(FeMn)$ and $Al_6(FeMn)$ is higher than that of α-Fe [9]. According to the Refs. [8,20], the formation temperature of $Al_3(FeMn)$ and $Al_6(FeMn)$ is both above 640 °C, but the liquidus temperature of the alloy with 1.1% Si is 649.6 °C. Because of the relatively high cooling rate during the die casting, the formation of the $Al_3(FeMn)$ and $Al_6(FeMn)$ can be suppressed. Thus, there are more free available Fe atoms for the formation of α-Fe.

3.2 Tensile properties

Figure 11 shows the effect of applied pressure and Si content on the tensile properties of the alloys. It is worth emphasizing that an increase in applied pressure brings about a significant improvement in the strength and elongation of Al−5.0Cu−0.6Mn−1.2Fe alloys. For the alloys without the addition of Si, when the applied pressure increases from 0 to 75 MPa, the UTS of the alloys increases from 206 to 223 MPa, the YS increases from 109 to 114 MPa and the elongation increases from 6.1% to 11.7%. This result is consistent with previous study [35]. The increments of UTS, YS and elongation of the alloys are about 8.1%, 4.6%, and 93.1%, respectively. Similarly, for the alloys with addition of 1.1% Si, when the applied pressure increases from 0 to 75 MPa, the UTS, YS and elongation are further increased by 35.2%, 40.0%, and 140.2%, respectively.

The fracture surface morphologies of the alloys with different Si contents are shown in Fig. 12. The fracture surfaces of the Si-free alloys without applied pressure (Figs. 12(a) and (b)) show many large porosities (~50 μm) and high volume fraction of secondary phases at grain boundaries, leading to many tearing ridges. As the applied pressure is increased to 75 MPa, some dimples but no porosity are found on the fracture surface (Figs. 12(c) and (d)), which implies that the applied pressure tends to improve the ductility. The fracture surface of the alloy with 1.1% Si produced without applied pressure shows the porosities and microcracks and the cracks propagate along the interface between large α-Fe and α(Al) (Figs. 12(e) and (f)). For the samples with applied pressure of 75 MPa, the fracture morphology of integrated α-Fe and Al_2Cu phases shows the feature of quasi-cleavages, as seen in Figs. 11(g) and (h). In order to further understand the failure mechanism,

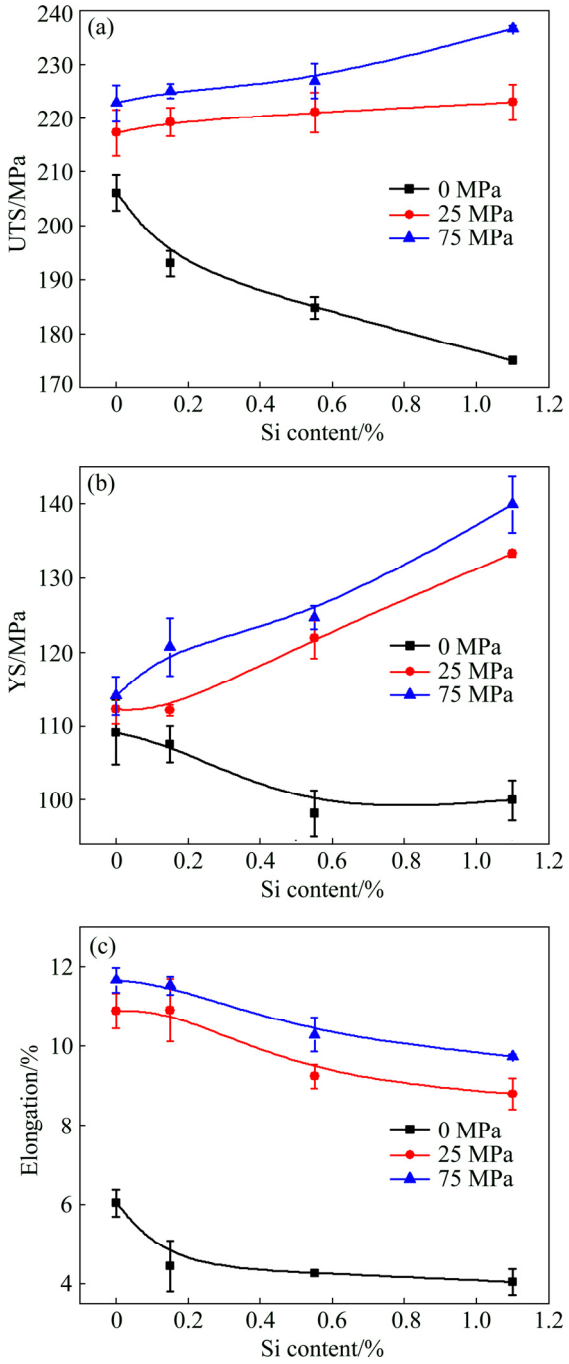

Fig. 11 Mechanical properties of alloys at different Si contents and applied pressures: (a) UTS; (b) YS; (c) Elongation

the longitudinal microstructures beneath the fracture surfaces of the alloys are shown in Fig. 13. The secondary phases and porosities are the preferable locations for the crack initiation and propagation (Figs. 13(a) and (c)), while cracks are mainly concentrated on refined and compact α-Fe for the samples produced by squeeze casting (Figs. 13(b) and (d)).

As described above, the strength and elongation of the alloys increase with increasing applied pressure at the same level of Si content, which could be deduced from

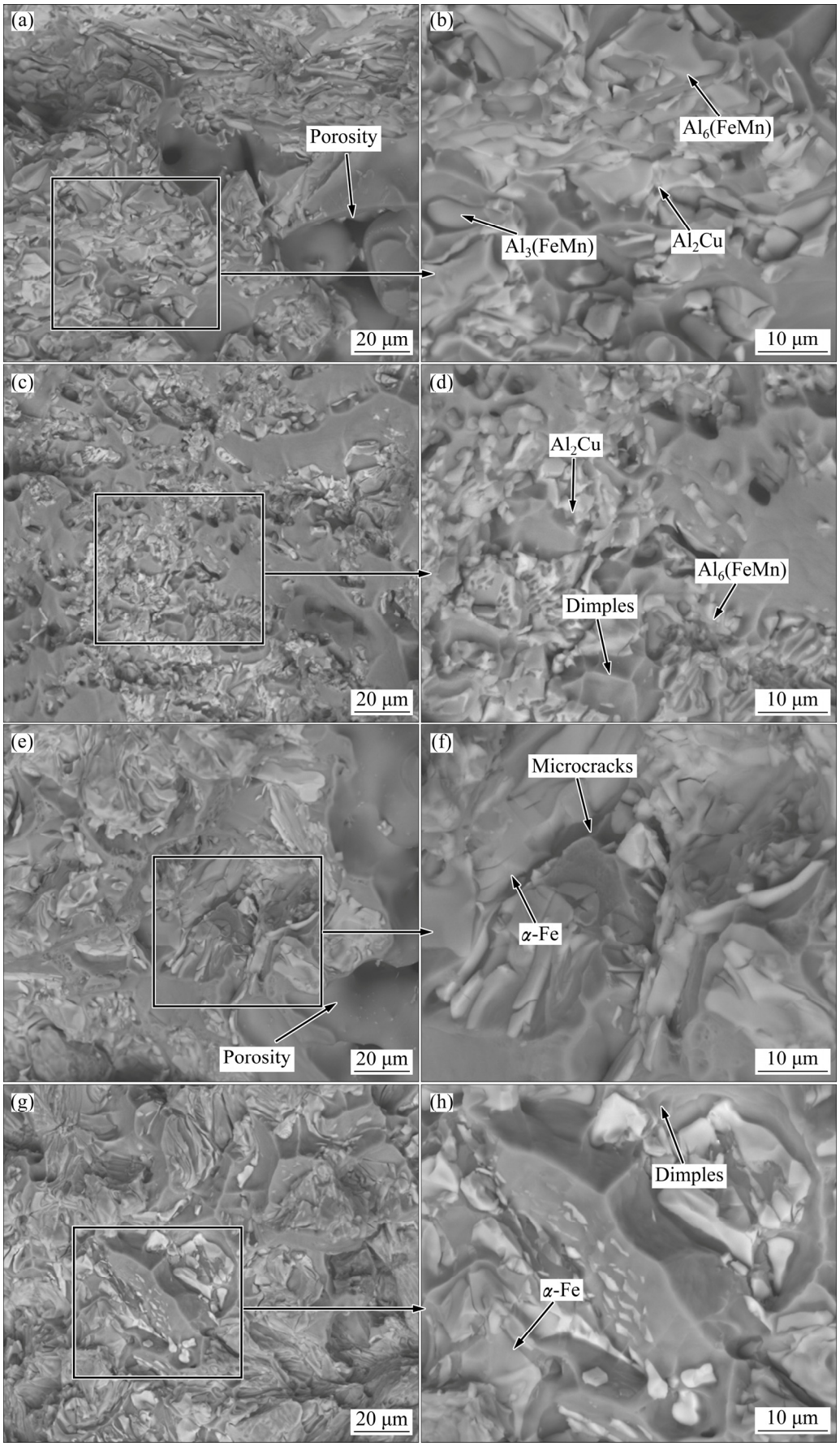

Fig. 12 Fracture surface morphologies of alloys with different Si contents and applied pressures: (a, b) 0% Si, 0 MPa; (c, d) 0% Si, 75 MPa; (e, f) 1.1% Si, 0 MPa; (g, h) 1.1% Si, 75 MPa

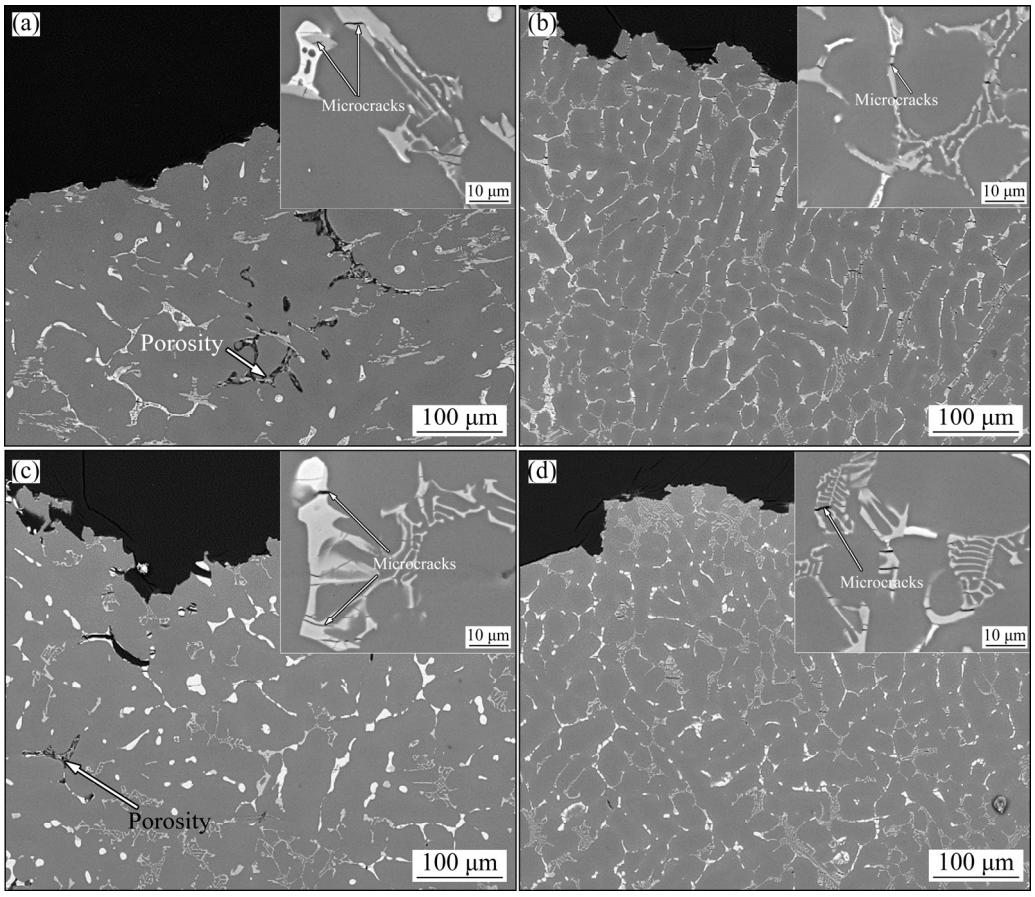

Fig. 13 Microstructures beneath fracture surfaces of alloys at different applied pressures and silicon contents: (a) 0%Si, 0 MPa; (b) 0%Si, 75 MP; (c) 1.1%Si, 0 MPa; (d) 1.1%Si, 75 MPa

the grain refinement strengthening, solid-solution strengthening and elimination of porosity. First, the average grain size of the alloy under 75 MPa applied pressure decreases compared with that of the alloy without applied pressure. Also, the solid-solution strengthening is contributed to the increasement of the strength [37]. The solubility of the alloying elements in the α(Al) matrix is presented in Table 3 and the microhardness of the solid-solution matrix was measured, as displayed in Fig. 14. Taking 1.1% Si alloy for example, as the applied pressure increases from 0 to 75 MPa, the hardness of α(Al) matrix increases from HV 64.4 to HV 75.7 and the solubility of Cu in α(Al) matrix increases from 1.24% to 2.59% (molar fraction). These imply that the applied pressure makes higher amount of Cu dissolve in the α(Al) matrix, leading to the solid-solution strengthening [38,39]. In addition, the elimination of porosity partially contributes to the improvement of strength.

The UTS, YS and elongation of the alloys decrease with increasing Si content when the alloys are produced without applied pressure. The increasing amount of porosity and Fe-rich intermetallics plays a leading role in the deterioration of the tensile properties. As shown in

Table 3 Chemical compositions of α(Al) matrix in alloys

w(Si)/%	Applied pressure/MPa	w(Cu)/%	w(Mn)/%	w(Fe)/%	w(Si)/%
0	0	1.09	0.48	0.07	0.02
	75	2.54	0.51	0.10	0.02
1.1	0	1.24	0.47	0.09	0.14
	75	2.59	0.48	0.09	0.27

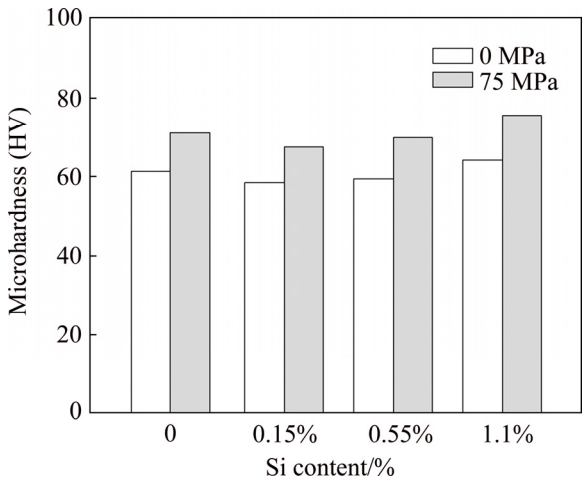

Fig. 14 Microhardness of α(Al) matrix in different alloys

Fig. 4, the porosity increases as the Si content increases. The cracks easily initiate and propagate along the porosity, resulting in the decreasing of UTS and YS. The increasing amount of Fe-rich intermetallics prevents liquid feeding and promotes formation of porosity in the solidification. The site of porosity and coarse Fe-rich intermetallics are apt to be the cracks initiation sites, as demonstrated in the fracture surface morphologies (Figs. 12(a) and (e)). It is interesting to note that the UTS, YS and elongation of the alloys increase slightly with increasing Si content when the alloys are produced at the applied pressure of 75 MPa. It is considered that Si addition promotes the formation of the Chinese script α-Fe and suppresses the formation of plate-like Al_3(FeMn) and Chinese script Al_6(FeMn), which is less harmful to the tensile properties. The Chinese script α-Fe is usually interwoven with α(Al), making the crack more difficult to propagate. These are also confirmed by the cracks propagation through the arms of α-Fe in multi-directions (Figs. 11(e) and (g)) and the broken Fe-rich intermetallics (Figs. 12(b) and (d)). And the applied pressure makes the Fe-rich intermetallics tend to be refined and compact, which could strengthen the alloy by acting as pins to prevent dislocations from sliding under stress. Also, Si enhances the strength of the alloys by increasing the number density of fine θ phase, because Si addition could accelerate the precipitation kinetics and increase coarsening resistance of the precipitates [31].

4 Conclusions

1) The Al−5.0Cu−0.6Mn−1.2Fe alloys show three kinds of Fe-rich intermetallics, i.e., Chinese script α-Fe, Al_6(FeMn) and platelet-like Al_3(FeMn). Si addition promotes the formation of less harmful α-Fe and suppresses the formation Al_3(FeMn) and Al_6(FeMn).

2) The applied pressure significantly improves the strength of the alloys, which is attributed to the elimination of porosity, grain refinement strengthening and solid-solution strengthening. The UTS and YS of the alloys produced at 75 MPa increases obviously with increasing Si content, while the UTS and YS decrease without applied pressure, because the Si addition promotes the formation of compact α-Fe and the precipitation of refined and high number density θ phases under applied pressure.

3) The alloy with addition of 1.1% Si produced under the applied pressure of 75 MPa shows the best tensile properties, where the UTS, YS and elongation are 237 MPa, 140 MPa and 9.8%, respectively, which are 35.2%, 40.0%, and 140.2% higher than those of the counterpart without applied pressure, respectively.

References

[1] WANG Zhi, QU Rui-tao, SCUDINO S, SUN Bao-an, PRASHANTH K G, LOUZGUINE-LUZGIN D V, CHEN Ming-wei, ZHANG Zhe-feng, ECKERT J. Hybrid nanostructured aluminum alloy with super-high strength [J]. NPG Asia Materials, 2015, 7: 1−8.

[2] HARRIGAN W C. Handbook of metallic composites [M]. New York: Marcel Dekker, 1994.

[3] BROWN J. Foseco non-ferrous foundryman's handbook [M]. Oxford: Butterworth-Heinemann, 1999.

[4] GREEN J A S. Aluminum recycling and processing for energy conservation and sustainability [M]. Materials Park, OH: ASM International, 2007.

[5] ZHANG, Li-feng, GAO Jian-wei, LUCAS N W D, ROBERTSON D G. Removal of iron from aluminum: A review [J]. Mineral Processing and Extractive Metallurgy Review, 2012, 33: 99−157.

[6] KAUFMAN J G, ROOY E L. Aluminum alloy castings: Properties, processes, and applications [M]. Materials Park, OH: ASM International, 2004.

[7] MONDOLFO L F. Aluminum alloys: structure and properties [M]. London: Butterworths, 1976.

[8] LIU K, CAO X, CHEN X G. Formation and phase selection of iron-rich intermetallics in Al−4.6Cu−0.5Fe cast alloys [J]. Metallurgical and Materials Transactions A, 2013, 44: 682−695.

[9] LIU K, CAO X, CHEN X G. Precipitation of iron-rich intermetallic phases in Al−4.6Cu−0.5Fe−0.5Mn cast alloy [J]. Journal of Materials Science, 2012, 47: 4290−4298.

[10] ALLENA C M, O'REILLYA K A, CANTORA B, EVANSB P V. Intermetallic phase selection in 1XXX Al alloys [J]. Progress in Materials Science, 1998, 43: 89−170.

[11] LIU K, CAO X, CHEN X G. A new iron-Rich intermetallic-Al_mFe phase in Al−4.6Cu−0.5Fe cast alloy [J]. Metallurgical and Materials Transactions A, 2012, 43: 1097−1101.

[12] LIN Bo, ZHANG Wei-wen, ZHAO Yu-liang, LI Yuan-yuan. Solid-state transformation of Fe-rich intermetallic phases in Al−5.0Cu−0.6Mn squeeze cast alloy with variable Fe contents during solution heat treatment [J]. Materials Characterization, 2015, 104: 124−131.

[13] ZHANG Wei-wen, LIN Bo, ZHANG Da-tong, LI Yuan-yuan. Microstructures and mechanical properties of squeeze cast Al−5.0Cu−0.6Mn alloys with different Fe content [J]. Materials and Design, 2013, 52: 225−233.

[14] LIN Bo, ZHANG Wei-wen, LOU Zhao-hui, ZHANG Da-tong, LI Yuan-yuan. Comparative study on microstructures and mechanical properties of the heat-treated Al−5.0Cu−0.6Mn−xFe alloys prepared by gravity die casting and squeeze casting [J]. Materials and Design, 2014, 59: 10−18.

[15] KAMGA H K, LAROUCHE D, BOURNANE M, RAHEM A. Mechanical properties of aluminum-copper B206 alloys with iron and silicon additions [J]. International Journal of Cast Metals Research, 2012, 25: 15−25.

[16] ZHANG Wei-wen, LIN Bo, CHENG Pei, ZHANG Da-tong, LI Yuan-yuan. Effects of Mn content on microstructures and mechanical properties of Al−5.0Cu−0.5Fe alloys prepared by squeeze casting [J]. Transactions of Nonferrous Metals Society of China, 2013, 23: 1525−1531.

[17] LIU K, CAO X, CHEN X G. Solid-state transformation of iron-rich intermetallic phases in Al-Cu 206 cast alloys during solution heat treatment [J]. Metallurgical and Materials Transactions A, 2013, 44: 3494−3503.

[18] BELOV N A, AKSENOV A A, ESKIN D G. Iron in aluminum alloys: Impurity and alloying element [M]. London: CRC Press, 2002.

[19] TSENG C J, LEE S L, TSAI S C, CHENG C J. Effects of manganese on microstructure and mechanical properties of A206 alloys containing iron [J]. Journal of Materials Research, 2002, 17: 2243−2250.
[20] LIU K, CAO X, CHEN X G. Effect of Mn, Si, and cooling rate on the formation of iron-rich intermetallics in 206 Al−Cu cast alloys [J]. Metallurgical and Materials Transactions A, 2012, 43: 1231−1240.
[21] LIU K, CAO X, CHEN X G. Solidification of iron-rich intermetallic phases in Al−4.5Cu−0.3Fe cast alloy [J]. Metallurgical and Materials Transactions A, 2011, 42: 2005−2016.
[22] KAMGA H K, LAROUCHE D, BOURNANE M, RAHEM A. Solidification of aluminum-copper B206 alloys with iron and silicon additions [J]. Metallurgical and Materials Transactions A, 2010, 41: 2845−2855.
[23] KAMGA H K, LAROUCHE D, BOURNANE M, RAHEM A. Hot tearing of aluminum-copper B206 alloys with iron and silicon additions [J]. Materials Science and Engineering A, 2010, 527: 7413−7423.
[24] TALAMANTES-SILVA M A, RODRIGUEZ A, TALAMANTES-SILVA J, VALTIERRA S, COLÁS R. Characterization of an Al−Cu cast alloy [J]. Materials Characterization, 2008, 31: 1434−1439.
[25] LEMIEUX A, LANGLAIS J, BOUCHARD D, CHEN X G. Effect of Si, Cu and Fe on mechanical properties of cast semi-solid 206 alloys [J]. Transactions of Nonferrous Metals Society of China, 2010, 20: 1555−1560.
[26] HAN N, BIAN X F, LI Z K, MAO T, WANG C D. Effect of Si on the microstructure and mechanical properties of the Al−4.5% Cu alloys [J]. Acta Metallurgica Sinica, 2006, 19: 405−410.
[27] GHOMASHCHI M R, VIKHROV A. Squeeze casting: An overview [J]. Journal of Materials Processing Technology, 2000, 101: 1−9.
[28] LI Yuan-yuan, ZHANG Wei-wen, ZHAO Hai-dong, YOU Dong-dong, ZHANG Da-tong, SHAO Ming, ZHANG Wen. Research progress on squeeze casting in China [J]. China Foundry, 2014, 11: 239−246.
[29] YUE T M. Squeeze casting of high-strength aluminium wrought alloy AA7010 [J]. Journal of Materials Processing Technology, 1997, 66: 179−185.
[30] ZHANG Yang, LI Feng-lei, LUO Zhi, ZHAO Yu-liang, XIA Wei, ZHANG Wei-wen. Effect of applied pressure and ultrasonic vibration on microstructure and microhardness of Al−5.0Cu alloy [J]. Transactions of Nonferrous Metals Society of China, 2016, 26: 2296−2303.
[31] ZHENG Cheng-kun, ZHANG Wei-wen, ZHANG Da-tong, LI Yuan-yuan. Low cycle fatigue behavior of T4-treated Al−Zn−Mg−Cu alloys prepared by squeeze casting and gravity die casting [J]. Transactions of Nonferrous Metals Society of China, 2015, 25: 3505−3514.
[32] ZHANG Wei-wen, LIN Bo, FAN Jian-lei, ZHANG Da-tong, LI Yuan-yuan. Microstructures and mechanical properties of heat-treated Al−5.0Cu−0.5Fe squeeze cast alloys with different Mn/Fe ratio [J]. Materials Science and Engineering A, 2013, 588: 366−375.
[33] VO N Q, DUNAND D C, SEIDMAN D N. Improving aging and creep resistance in a dilute Al−Sc alloy by microalloying with Si, Zr and Er [J]. Acta Materialia, 2014, 63: 73−85.
[34] MITLIN D, MORRIS J W, RADMILOVIC V. Catalyzed precipitation in Al−Cu−Si [J]. Metallurgical and Materials Transactions A, 2000, 31: 2697−2711.
[35] WANG E R, HHI X D, WANG S S, ZHAO Y F, CHEN G L. Improved mechanical properties in cast Al–Si alloys by combined alloying of Fe and Cu [J]. Materials Science and Engineering A, 2010, 527: 7878−7884.
[36] BELOV N A. Quantitative analysis of the primary crystallization of iron-containing phases as applied to aluminum alloys of various doping systems [J]. Russian Journal of Non-Ferrous Metals, 2013, 54: 300−306.
[37] ZHANG Wei-wen, LIN Bo, LUO Zhi, ZHAO Yu-liang, LI Yuan-yuan. Formation of Fe-rich intermetallic compounds and their effect on the tensile properties of squeeze-cast Al−Cu alloys [J]. Journal of Materials Research, 2015, 30: 2474−2484.
[38] SOBCZAK J J, DRENCHEV L, ASTHANA R. Effect of pressure on solidification of metallic materials [J]. International Journal of Cast Metals Research, 2012, 25: 1−14.
[39] EL-KHAIR M A. Microstructure characterization and tensile properties of squeeze-cast AlSiMg alloys [J]. Materials Letters, 2005, 59: 894−900.

Si 添加和压力对铸造 Al−5.0Cu−0.6Mn−1.2Fe 合金组织和力学性能的影响

张卫文，赵愈亮，张大童，罗宗强，杨 超，李元元

华南理工大学 国家金属材料近净成形工程技术研究中心，广州 510641

摘 要：研究 Si 添加和压力对铸造 Al−5.0Cu−0.6Mn−1.2Fe 合金显微组织和力学性能的影响。结果表明，添加 Si 可促进 α-Fe 的形成，并抑制 $Al_3(FeMn)$和 $Al_6(FeMn)$的形成。对于重力铸造的合金，添加 Si 会增加孔洞的体积分数，导致合金的抗拉强度(UTS)和屈服强度(YS)显著降低。对于在 75 MPa 压力下制备的合金，Si 添加促进高密度 Al_2Cu (θ)相的形成，从而使抗拉强度和屈服强度增加。在相同 Si 含量的合金中，力学性能随施加压力的增加而增加，这是由于孔洞减少、晶粒细化强化和固溶强化所致。合金最好的力学性能出现在压力为 75 MPa 和 Si 含量为 1.1%时，其 UTS、YS 和伸长率分别为 237 MPa、140 MPa 和 9.8%。

关键词：铝铜合金；硅添加；凝固；力学性能；显微组织

(Edited by Bing YANG)